Research article

Daria I. Markina, Anatoly P. Pushkarev*, Ivan I. Shishkin, Filipp E. Komissarenko, Alexander S. Berestennikov, Alexey S. Pavluchenko, Irina P. Smirnova, Lev K. Markov, Mikas Vengris, Anvar A. Zakhidov and Sergey V. Makarov*

Perovskite nanowire lasers on low-refractive-index conductive substrate for high-Q and low-threshold operation

https://doi.org/10.1515/nanoph-2020-0207
Received March 24, 2020; accepted May 11, 2020; published online June 24, 2020

Abstract: Over the last five years, inorganic lead halide perovskite nanowires have emerged as prospective candidates to supersede standard semiconductor analogs in advanced photonic designs and optoelectronic devices. In particular, $CsPbX_3$ (X = Cl, Br, I) perovskite materials have great advantages over conventional semiconductors such as defect tolerance, highly efficient luminescence, and the ability to form regularly shaped nano- and microcavities from solution via fast crystallization. However, on the way of electrically pumped lasing, the perovskite nanowires grown on transparent conductive substrates usually suffer from strong undesirable light leakage increasing their threshold of lasing. Here, we report on the integration of $CsPbBr_3$ nanowires with nanostructured indium tin oxide substrates possessing near-unity effective refractive index and high conductivity by using a simple wet chemical approach. Surface passivation of the substrates is found out to govern the regularity of the perovskite resonators' shape. The nanowires show room-temperature lasing with ultrahigh quality factors (up to 7860) which are up to four times higher than that of similar structures on a flat indium tin oxide layer, resulting in more than twofold reduction of the lasing threshold for the nanostructured substrate. Numerical modeling of eigenmodes of the nanowires confirms the key role of low-refractive-index substrate for improved light confinement in the Fabry–Pérot cavity which results in superior laser performance.

Keywords: $CsPbBr_3$; Fabry–Pérot cavity; lasing; nanolaser; nanowire; perovskite; ultrahigh quality factor.

***Corresponding authors: Anatoly P. Pushkarev and Sergey V. Makarov**, Department of Physics and Engineering, ITMO University, St. Petersburg, 197101, Russia,
E-mail: anatoly.pushkarev@metalab.ifmo.ru (Anatoly P. Pushkarev); and E-mail: s.makarov@metalab.ifmo.ru (Sergey V. Makarov).
https://orcid.org/0000-0002-9257-6183 (S.V. Makarov)
Daria I. Markina, Ivan I. Shishkin, Filipp E. Komissarenko and Alexander S. Berestennikov: Department of Physics and Engineering, ITMO University, St. Petersburg, 197101, Russia. https://orcid.org/0000-0002-3846-0569 (D.I. Markina)
Alexey S. Pavluchenko, Irina P. Smirnova and Lev K. Markov: Ioffe Institute, St. Petersburg, 194021, Russia
Mikas Vengris: Laser Research Center, Faculty of Physics, Vilnius University, Vilnius, LT-10223, Lithuania
Anvar A. Zakhidov: Department of Physics and Engineering, ITMO University, St. Petersburg, 197101, Russia; University of Texas at Dallas, Richardson, TX, 75080, USA

1 Introduction

Nowadays, new platforms and concepts in material science, solid-state physics, and engineering have been emerged due to halide perovskites. A rapid progress in the power conversion efficiency from 3.8 to 25.2% of perovskite-based solar cells [1, 2] stimulated enormous interest to ABX_3 (A = MA^+ – methylammonium, FA^+ – formamidinium, Cs^+; B = Pb^{2+}; X = Cl^-, Br^-, I^-) materials for the development of various optoelectronic devices [3–5], optically pumped microlasers [6–9] and other photonic designs enabling efficient light management at nanoscale [10–13]. All-inorganic $CsPbX_3$ perovskites are good candidates to be applied for various nanophotonic applications [14, 15] since they are not as sensitive to moisture as their organic–inorganic counterparts and tend to form regularly shaped cavities from precursor solution at moderate temperatures of 50–70 °C. In particular, both optical gain (~10^4 cm^{-1} [16–18]) and refractive index (2–2.5) of the medium are high enough to create ultracompact lasers [19, 20]. Remarkably, in terms of the directivity of coherent light output, nanowires (NWs) emitting in two opposite directions have an advantage over whispering gallery mode polygons [6, 21], discs [9], spheres [7], and Mie-resonant nanoparticles [16] that need to be coupled with an external bus waveguide

[22]. Additionally, perovskite NWs can be easily connected with electrodes [23] aiming to achieve electrically driven lasing which is still elusive [24]. Indeed, first of all, it is crucial to provide high optical contrast between the microlaser and substrate to achieve strong optical gain amplification [25], high quality factor (Q-factor) and, thus, low lasing threshold preventing the laser overheating. The increase in the Q-factor can be achieved by the integration of the NWs with low-refractive-index substrate providing high dielectric contrast between the active media and the environment and, thus, suppressing the light leakage into the substrate. However, creation of low-index substrates with good conductance as well as growing perovskite NWs on them are challenging.

In this work, we propose a conductive substrate with near-unity refractive index for improvement of photophysical properties of inorganic perovskite nanowire lasers. Namely, we demonstrate significant reduction of the lasing threshold and ultrahigh Q-factors of lasing modes in few micrometers length $CsPbBr_3$ NWs integrated with the nanostructured indium tin oxide (NS ITO) substrate possessing an effective refractive index of ≈ 1.15, sheet resistance of ≈ 60 Ohm/sq, and low chemical reactivity with the $CsPbBr_3$ material. The developed approach results in the reduction of laser modes leakage and opens up new opportunities for the engineering of ultracompact and high-Q nanophotonic designs placed on transparent and conductive layers which is prospective for electrically pumped light-emitting architectures.

2 Results and discussion

2.1 Samples fabrication and characterization

Nanostructured ITO films consisting of out-of-plane randomly oriented nanowhiskers (Figure S1) were formed on a compact ITO layer by electron-beam evaporation (for details, see Section 4). The films thickness was about 650 nm. During the deposition, nuclei on the surface of the compact layer rapidly evolve into whiskers of tens nm in diameter. The formation of wire-like ITO crystals occurs via a vapor–liquid–solid synthesis [26, 27]. In this self-catalytic process, the crystal growth happens at the solid–liquid interface between the ITO crystal and a droplet of In–Sn alloy sitting at the end facet of the crystal. Initially, In and Sn condense on a hot substrate in the form of a nanoscale droplet. When the droplet reacts with oxygen, an ITO seed crystal nucleates on its surface and precipitates. Although the seed crystals grow along [001] direction, their [001] crystallographic axis is not always orthogonal to the substrate surface, because of the random orientation of the precipitated seed crystals with respect to the substrate surface. As a result, different ITO nanowhiskers grow in different spatial directions, and, during this process, vertically aligned nanowhiskers "shade" the tilted ones and slow down their growth. For this reason, the density of the nanostructured layer gradually decreases with the distance (h) from the substrate surface, and hence the effective refractive index (n_{eff}) of the layer decreases as well. The profile $n_{eff}(h)$ at λ = 530 nm was derived from numerical calculations of the transmittance and reflectance spectra using the transfer-matrix method [28]. Figure S1 shows that n_{eff} = 1.93 at h = 0 nm, whereas it takes values close to unity when the height exceeds 550 nm. Taking into consideration that perovskite cavity could efficiently interact at least with 400 nm of underlying NS ITO via an evanescent field, the value of n_{eff} = 1.15 can be roughly employed to demonstrate an impact of the excellent optical contrast between NS ITO and $CsPbBr_3$ NW (n = 2.3) on laser performance of the latter. Furthermore, since conductive oxide substrates are commonly exploited for the charge injection in various optoelectronic devices it is worth noting that the measured sheet resistance (R_S) of our NS ITO films is around 60 Ohm/sq. This makes them good candidates for the engineering of electrically driven light-emitting structures.

To produce $CsPbBr_3$ NWs we use a simple and scalable solution-phase approach – rapid precipitation of nano- and microcrystals from a perovskite ink droplet. A droplet containing $PbBr_2$ and CsBr mixed in 1:1 stoichiometric ratio in anhydrous dimethyl sulfoxide (DMSO) is deposited on hydrophobic substrate and exposed to 2-propanol-water ($IPA{\cdot}H_2O$) azeotropic vapor for a short time at 50 °C (Figure 1a; for details, see Section 4). The mechanism of NWs formation is described in our previous report [29]. It was established that ionic species (it could be $[(CH_3)_2CHO]^-$–$[H_3O]^+$ pair or $[(CH_3)_2CHOH_2]^+$–$[OH]^-$ one) generated due to reversible proton transfer between water and IPA ($(CH_3)_2CHOH$) molecules act as capping ligands for $CsPbBr_3$ seed crystals. These ligands passivate surface of nanocrystals of few nm size that otherwise would agglomerate yielding a polycrystalline sediment. Dynamic absorption and release of the ionic ligands by the seed crystals occurring in the presence of perovskite precursors enables the in situ crystallization process. As a result, separate monocrystalline NWs adopting an orthorhombic structure are formed on the substrate [29].

For cultivation of perovskite NWs on NS ITO layer, the substrate should be soaked in some hydrophobic substance to fill in the void space between nanowhiskers. Oleic acid (OA) dissolved in toluene was found to be suitable for

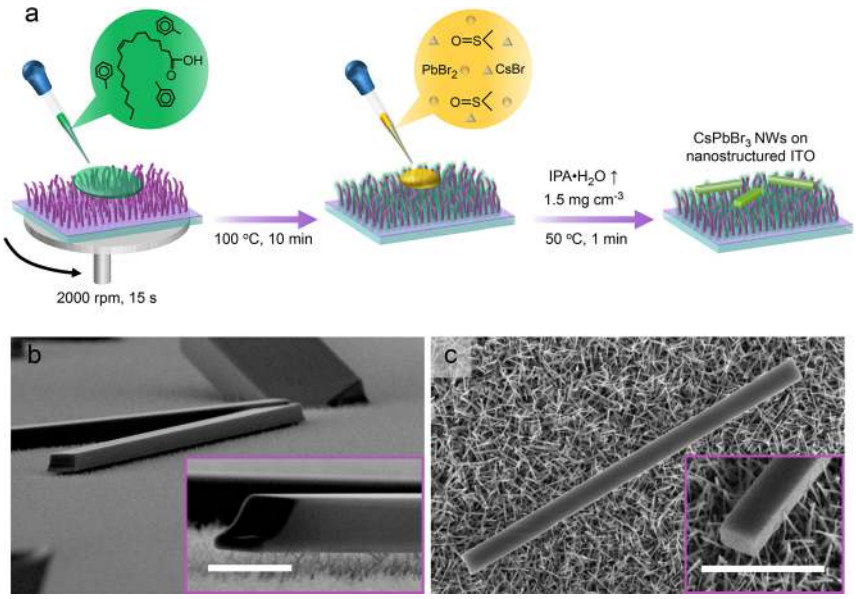

Figure 1: (a) Schematic representation of the process of perovskite NWs cultivation on nanostructured ITO substrate. (b, c) SEM images of typical $CsPbBr_3$ micro- and nanostructures obtained for the ITO substrate covered with oleic acid (OA) from 3 (b), and 5 wt. % (c) toluene solution (scale bars are 1 μm). One can see that 3 wt. % solution gives microwires having more or less regular shape however their end facets are distorted. Increase in OA content up to 5 wt. % results in reducing the substrate wettability and evolution of the end facets shape from distorted to rectangular.

this purpose. Spin-casting of the solution and drying the deposited film at 100 °C provides the substrate with hydrophobicity (Figure 1a). Importantly, the subsequent deposition of NWs on the passivated substrate has to be a short-term procedure which takes approximately 1 min (for details, see Section 4). When the deposition lasts remarkably longer, no perovskite cavities having a regular shape are obtained. This could be explained by the dissolving of OA protective layer with DMSO. As a result numerous centers (nanowhiskers) for the perovskite crystallization appear, and hence the formation of the polycrystalline sediment happens. To study the influence of the NS ITO passivation on the size and shape of $CsPbBr_3$ crystals the toluene solutions containing 0, 1, 3 and 5 wt. % of OA were spin-casted on the substrates. The absence of the passivating agent leads to the formation of perovskite micro-objects having irregular shape (Figure S2a, b and c). 1 wt. % solution gives microwires and microplates with facets wetting the substrate (Figure S2d and e). 3 wt. % solution affords the formation of microwires possessing more or less regular end facets (Figures 1b and S2f and g). Finally, when concentration of the acid in toluene increases up to 5 wt. % we obtain almost free standing Fabry–Pérot (F–P) cavities (Figures 1c and S2h–l).

2.2 Optical properties

Among the crucial optical characteristics of a laser source there are two the most commonly demonstrated. The first one is the lasing threshold (F_{th}), which determines the value of incident fluence from pulsed optical pump inducing coherent emission. This value should be as low as possible to reduce photodegradation of the gain medium. The second one is full width at half maximum (FWHM or $\delta\lambda$) of the stimulated emission peaks. Minimization of FWHM in miniature on-chip lasers paves the way to high-speed multichannel photonic integrated circuits [30] and ultrafine optical sensors [31]. In fact, $\delta\lambda$ can be very small when the resonator shows high energy stored-to-power loss ratio. In laser condition, this ratio is proportional to lasing Q-factor (Q_{las}) that can be deduced from Schawlow–Townes equation corrected by Lax as [32]:

$$Q_{las} = \frac{\lambda}{\delta\lambda} = \frac{P_{out} Q_{cav}^2 \lambda^2}{2\pi^2 hc^2}, \quad (1)$$

where λ is a laser line central wavelength, c – speed of the light, h – the Plank constant, P_{out} is the laser output power, and Q_{cav} is the cavity quality factor which is given by the formula [33]:

$$\frac{1}{Q_{cav}} = \frac{1}{Q_{abs}} + \frac{1}{Q_{leak}} + \frac{1}{Q_{scat}}. \quad (2)$$

Herein, Q_{abs}, Q_{leak}, and Q_{scat} define absorption, leakage, and scattering losses, respectively.

In our study, we address an issue of the leakage loss in the perovskite NW caused by the field leakage out of the cavity into high-index conductive oxide substrate. To estimate a positive impact of the low-index nanostructured ITO layer on optical performance of perovskite NWs the photoluminescent (PL) behavior of 8.9 μm NW **1** deposited on NS ITO was compared with that of 9 μm NW **2** lying on a

flat ITO layer (Figure 2a and b). Although the cross-sectional dimensions of the NWs are not the same, this should not affect spectral characteristics since quality factor of F–P cavity is mainly determined by its length [34]:

$$Q_{cav}^{FP} = -\frac{Lk_{||}}{\ln|R_1R_2|}, \quad (3)$$

where R_1 and R_2 the reflection coefficients at each facet, L is the NW length, and $k_{||}$ is the longitudinal projection of wavenumber along the NW axis. The optical properties of the NWs were investigated at ambient conditions. PL spectra were measured under 349 nm fs pulsed laser excitation (for details, see Section 4).

At low fluence, both NWs exhibit broadband ($\delta\lambda$ = 16 nm) spontaneous emission at ca. 526 nm (Figure S3). Above the lasing threshold, sharp peaks appear on the low-energy side of the emission spectrum in the 534–544 nm region and grow with increase in pumping power. A coherent nature of the output signal collected from two end facets of single NW when $F > F_{th}$ is confirmed by the interference pattern observed in the experiments (see insets in Figure S3). Figure 2c and d illustrate how the FWHM of the most intensive peak in PL spectrum depends on fluence as well as integrated PL intensity versus fluence for NWs **1** and **2**, respectively. The lasing threshold for the NW on NS ITO substrate was found to be two times lower than that of the NW on flat ITO. $\delta\lambda$ values measured at two laser peaks in the PL spectrum of NW **2** fall within 0.3–0.4 nm range, whereas FWHM of six lines in the spectrum of NW **1** varies from 0.07 to 0.1 nm (Figure 2e and f). Thus integrating a perovskite nanolaser with a low-index ITO substrate not only results in a substantial reduction of the width of laser peaks as compared to that of nanolaser on flat ITO substrate, but it also enriches the emission spectrum with additional modes. The latter do not experience strong leakage loss, and hence survive in the cavity and can compete with the dominant laser modes.

Lineshape analysis of the stimulated emission spectra revealed that each of six laser modes of **1** perfectly matches a Gaussian function. On the contrary, every peak of **2** fits a double Gaussian distribution and consists of less intensive high- and more intensive low-energy components. The high-energy signals could correspond to emission from cold electron-hole plasma (EHP) which to some extent remains uncoupled with the field oscillating in the cavity (eigenmodes) (8). The absence of similar signals in the spectrum of **1** confirms the complete coupling between cold EHP and high-Q eigenmodes in the NW on low-index substrate. Indeed, maximal Q_{las} for the NW on NS ITO was estimated to be 7860 that exceeds 2–4 times the values established for $CsPbBr_3$ lasers of similar length on other

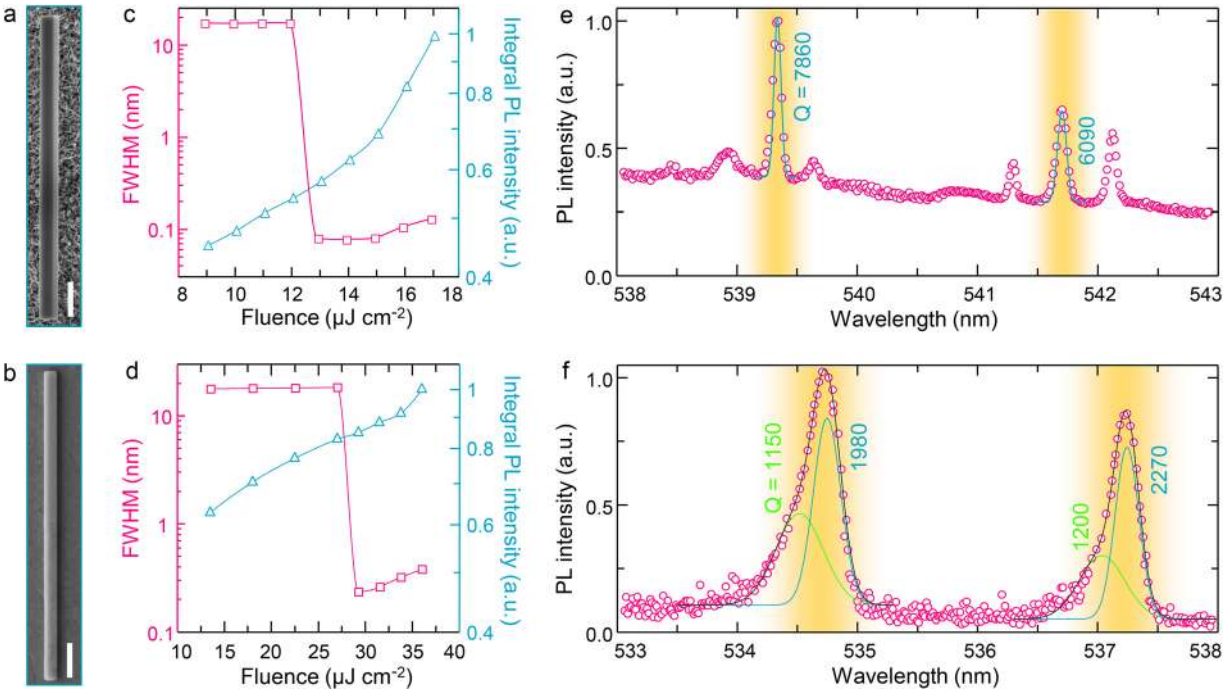

Figure 2: (a, b) SEM images of NW **1** on NS ITO and NW **2** on flat ITO, respectively (scale bars are 1 μm). (c, d) PL intensity and FWHM value versus excitation fluence for the nanowires. The laser threshold for NW **1** (c) is two times lower than that of NW **2** (d). (e, f) Q_{las}-factor analysis of the stimulated emission spectra observed for the NWs at the threshold fluence. For fitting the laser peaks, a Gaussian function is employed. NW **1** exhibits a four-fold increase in Q_{las} at dominant laser peak (e) as compared to that of the most intensive peak in the spectrum of NW **2** (f).

Table 1: Optical characteristics of $CsPbBr_3$ nanowire lasers of similar length deposited on various substrates.

Length (μm)	Threshold (μJ/cm^2)	Q_{las}^{max}	Substrate	Ref.
12	6.2	2070	glass	[35]
10.5	25	2265	glass	[29]
≈10	14.1	3500	SiO_2/Si	[36]
≈10	4	2256	M-plane Al_2O_3	[37]
9	28	2270	ITO	This work
8.9	13	7860	NS ITO	This work

substrates (Table 1) [29, 35–37]. We assume that such remarkable improvement of Q_{las} could stem from decent optical contrast between the NW (n = 2.3) and substrate (n_{eff} = 1.15) preventing the leakage loss. To confirm this assumption numerical simulations of the eigenmodes in NWs laying on substrates with different refractive indices are presented below.

It is also important to compare the temporal stability of laser operation for NWs on low- and high-refractive index substrates. For this purpose, the intensity of the dominant laser peak in the PL spectra of the samples operating under 1.2 F_{th} fluence at 40 kHz pulse repetition rate was measured for 15 min. Figure S4 shows very similar long-term stability for NWs on both substrates. However, a bit larger fluctuations in the peak intensity were found out for the NW on the flat ITO surface as compared to that of NW on the NS ITO. The reason for these fluctuations might be some photo- or thermal damages caused to the NW on the flat ITO by two times higher optical pumping.

2.3 Eigenmode simulations

Spectral and spatial characteristics of optical eigenmodes in a rectangular perovskite NW cavity lying on a dielectric infinite substrate with refractive index in the range of $n_{substrate}$ = 1.15…1.9, with special attention to the values 1.15, 1.9, and 1.5 corresponding to NS ITO, bulk ITO, and bulk glass, respectively, were analyzed by means of full-wave numerical simulations using a finite-element eigenmode-solver in COMSOL software (for details, see Section 4). Cavity quality factors (Q_{cav}) and electric field distribution were calculated near the lasing mode wavelength (535 ± 5 nm). The choice of the wavelength range is based on the values determined from our experiments. Since the modeling of the field distribution in 9 μm NW requires significant time costs and computing resources the geometric parameters of NW were set to be 3.5 × 0.4 × 0.4 μm that coincides with the dimensions of the smallest experimentally obtained NW laser (Figure S2i).

The results of the calculations show TM_{22} F–P mode profiles, namely E_Z component of electric field and absolute value of magnetic field |H| (Figure 3a–c) formed by back and forth light reflections, yielding the field structure corresponding to a standing wave between the two end facets. In order to investigate the field confinement η

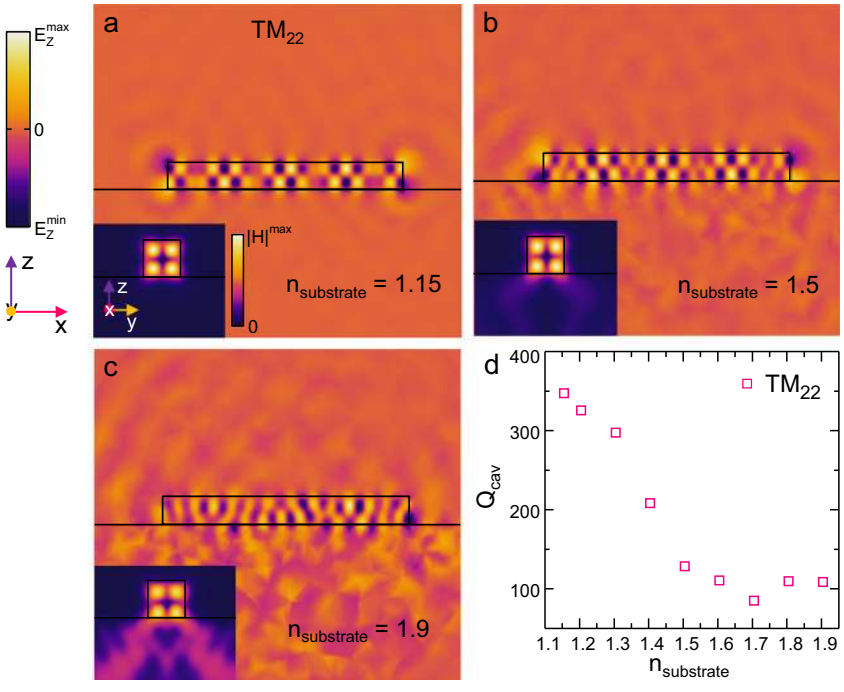

Figure 3: (a–c) Numerical modeling of the field spatial distribution of TM_{22} eigenmode in $CsPbBr_3$ cavity with 3.5 × 0.4 × 0.4 μm dimensions placed on substrates having different refractive indices: 1.15 (a), 1.5 (b), and 1.9 (c). E_Z component distribution is presented in the large-scale images, |H| – in the inset images. (d) Dependence of the cavity Q-factor calculated for TM_{22} eigenmode on the refractive index of the substrate.

in the NW, we calculate the ratio of the total energy time average inside NW (W_{NW}) to the total energy time average in the whole calculation cell (W_{cell}), $\eta = W_{NW}/W_{cell}$. It was revealed that NW on the flat ITO shows the worst field confinement ($\eta = 10\%$) as compared to NW on the NS ITO ($\eta = 82\%$) or glass substrate ($\eta = 56\%$). Additionally, we calculate Q-factors of eigenmodes ($Q_{cav} = \mathrm{Re}(\omega)/2|\mathrm{Im}(\omega)|$, where ω is the resonant frequency) depending on the substrate refractive index. Figure 3d shows a monotonic decrease in Q_{cav} from 350 down to ≈100 with an increase in the refractive index of the substrate from 1.15 up to 1.9. Thereby, the calculations verify the hypothesis of the Q-factor enhancement due to the substrate refractive index reduction and the prevention of optical mode leakage.

3 Conclusion

In summary, we have developed a novel type of conductive low-refractive-index substrates for integrating with solution-phase grown perovskite NW lasers to achieve excellent optical contrast. The substrates contain a nanostructured indium tin oxide (NS ITO) layer which has a near-unity refractive index ($n_{substrate} \approx 1.15$) improving light confinement in the optically active medium, and high conductivity ($R_S \approx 60$ Ohm/sq). As a result, we have demonstrated $CsPbBr_3$ NW exhibiting a laser mode with ultrahigh Q-factor of 7860 at low optical pumping threshold ($F_{th} = 13$ μJ/cm^2), being a record value among ones reported for perovskite NW lasers.

Significant Q-factor enhancement in perovskite nanowires that are Fabry–Pérot cavities and the gain media simultaneously extends the range of their exploitation as nanoscale coherent light sources. In particular, an increase in the lasing mode Q-factor enables hypersensitivity of the laser line to the environment changes such as the near-surface refractive index variation. It paves the way for the manufacturing of optical sensors analyzing the spectral response of a laser line in the presence of ultralow analyte concentrations in the surroundings [38]. Moreover, increasing the Q-factor of laser structures on a conductive substrate is extremely important for the development of electrically pumped deeply subwavelength nanolasers [16] and advanced high-Q microlasers [39], where the leakage of optical modes into the substrate might be almost eliminated. Finally, since NS ITO substrates are compatible with various methods of perovskite NWs fabrication [40, 41] we believe that our findings will give a boost to the development of novel applications of perovskite lasers for nanophotonics and optoelectronics.

4 Methods

4.1 Materials

Lead(II) bromide ($PbBr_2$, 99.999%, Alfa Aesar), cesium bromide (CsBr, 99.999%, Sigma-Aldrich), dimethyl sulfoxide (DMSO, anhydrous, 99.8%, Alfa Aesar), isopropyl alcohol (IPA, technical grade, 95%, Vecton), toluene (technical grade, Vecton), oleic acid (OA, technical grade, 90%, Vecton), and substrates with a flat ITO layer (350 nm) were purchased from commercial suppliers and used as received.

4.2 Preparation of perovskite ink solution

$PbBr_2$ (0.110 g, 0.3 mmol) and CsBr (0.063 g, 0.3 mmol) were mixed and dissolved in DMSO (3 ml) by shaking for 10 min to afford a clear solution. Then the solution was filtered by using a 0.45 μm syringe filter with a PTFE membrane. The chemicals were stored and mixed inside a N_2-filled glove box with both O_2 and H_2O level not exceeding 1 ppm.

4.3 NS ITO films fabrication

NS ITO films were produced by electron beam evaporation onto glass substrates heated up to 450 °C [42]. The deposition rate was set to 10 nm min^{-1}.

4.4 $CsPbBr_3$ nanowires deposition

Before the deposition, surface of the employed substrates was covered with a hydrophobic film of oleic acid spin-casted from its 1–5 wt. % toluene solutions at 2000 rpm for 15 s. Then the substrates were dried on a hot plate at 100 °C for 10 min to evaporate the residual solvent.

The diluted perovskite solution (0.1 M) was utilized at ambient conditions. The substrate with flat or NS ITO layer was fixed in a plastic Petri dish bottom (35 × 9 mm) placed in a bigger glass one (80 × 5 mm) and preheated on the hotplate up to 50 °C. A small droplet (0.5 μl) of the solution was dripped onto the substrate. Immediately after that, 200 μl of IPA·H_2O azeotrope was poured in the glass bottom and the big dish was sealed. When the droplet increased in size due to the condensation of IPA·H_2O azeotrope on its surface, the substrate was tilted in such a way that the droplet spread over the substrate leaving a trace. The trace was dried in the presence of the azeotropic vapor for 1 min to give isolated high-quality NWs.

4.5 Characterization

Morphology and size of the NWs were studied using a scanning electron microscope (Crossbeam 1540 XB, Carl Zeiss).

Spontaneous photoluminescence and lasing in a single NW were studied under 349 nm excitation with frequency doubled 150-fs pulses at 100 kHz repetition rate from an Yb-doped femtosecond laser (TeMa, Avesta Project). The beam was focused on the sample surface at normal incidence by a 10× microscope objective (Mitutoyo M Plan APO NIR, NA = 0.26) that was aligned to ensure uniform illumination of the NWs (Gaussian distribution with a FWHM of ≈ 20 μm). The emission of single NWs was collected from the top of 50× objective (Mitutoyo M

Plan APO NIR, NA = 0.42), sent to Horiba LabRam HR spectrometer, and projected onto a thermoelectrically cooled charge-coupled device (CCD, Andor DU 420A-OE 325). A parasitic signal corresponding to the excitation was blocked by a notch filter. Laser emission was studied by using a 1800 grooves/mm grating and a pinhole with 50 μm diameter at the entrance of the spectrometer. All measurements were performed at ambient conditions.

4.6 Eigenmode simulations

For numerical simulations of the eigenmode spectra of the resonator, we used the finite-element method in an eigenmode solver in COMSOL Multiphysics. All calculations are realized for a single NW of a certain size on a semiinfinite substrate surrounded by PML mimicking an infinite region. The values for the refractive index for $CsPbBr_3$ were taken from experimentally measured data for perovskite thin films [43] and increased by 0.25 to consider the high quality material structure [44] of fabricated monocrystalline NWs. The extinction coefficient is taken equal to zero for wavelengths longer than 530 nm, which allows to analyze the mode contribution in the lasing regime.

Acknowledgment: The authors are thankful to Kirill Koshelev for help with the numerical simulations. The numerical simulations were supported by the Ministry of Science and Higher Education (Project 14.Y26.31.0010). A.P. acknowledges Russian Science Foundation (Project 18-73-00346) for supporting the experimental part of the work. M.V. acknowledges the funding from the European Regional Development Fund according to the supported activity "Research Projects Implemented by World-class Researcher Groups" under Measure No. 01.2.2-LMT-K-718, grant No. 01.2.2-LMT-K-718-01-0014.

Author contribution: All the authors have accepted responsibility for the entire content of this submitted manuscript and approved submission.

Research funding: The work was funded by the Ministry of Science and Higher Education (Project 14.Y26.31.0010) and Russian Science Foundation (Project 18-73-00346). European Regional Development Fund (supported activity "Research Projects Implemented by World-class Researcher Groups" under Measure No. 01.2.2-LMT-K-718, grant No. 01.2.2-LMT-K-718-01-0014).

Conflict of interest statement: The authors declare no conflicts of interest regarding this article.

References

[1] A. Kojima, K. Teshima, Y. Shirai, and T. Miyasaka, "Organometal halide perovskites as visible-light sensitizers for photovoltaic cells," *J. Am. Chem. Soc.*, vol. 131, no. 17, pp. 6050–6051, 2009.

[2] https://www.nrel.gov/pv/assets/pdfs/best-research-cell-efficiencies.20190802.pdf.

[3] H. Wang, X. Zhang, Q. Wu, et al., "Trifluoroacetate induced small-grained cspbbr$_3$ perovskite films result in efficient and stable light-emitting devices," *Nat. Commun.*, vol. 10, no. 1, pp. 1–10, 2019.

[4] D. H. Chun, Y. J. Choi, Y. In, et al., "Halide perovskite nanopillar photodetector," *ACS Nano*, vol. 12, no. 8, pp. 8564–8571, 2018.

[5] W. Yu, F. Li, L. Yu, et al., "Single crystal hybrid perovskite field-effect transistors," *Nat. Commun.*, vol. 9, no. 1, pp. 1–10, 2018.

[6] Q. Zhang, S. T. Ha, X. Liu, T. C. Sum, and Q. Xiong, "Room-temperature near-infrared high-Q perovskite whispering-gallery planar nanolasers," *Nano Lett.*, vol. 14, no. 10, pp. 5995–6001, 2014.

[7] B. Tang, H. Dong, L. Sun, et al., "Single-mode lasers based on cesium lead halide perovskite submicron spheres," *ACS Nano*, vol. 11, no. 11, pp. 10681–10688, 2017.

[8] A. P. Schlaus, M. S. Spencer, K. Miyata, et al., "How lasing happens in $CsPbBr_3$ perovskite nanowires," *Nat. Commun.*, vol. 10, no. 1, pp. 1–8, 2019.

[9] A. Zhizhchenko, S. Syubaev, A. Berestennikov, et al., "Single-mode lasing from imprinted halide-perovskite microdisks," *ACS Nano*, vol. 13, no. 4, pp. 4140–4147, 2019.

[10] S. V. Makarov, V. Milichko, E. V. Ushakova, et al., "Multifold emission enhancement in nanoimprinted hybrid perovskite metasurfaces," *ACS Photon.*, vol. 4, no. 4, pp. 728–735, 2017.

[11] B. Gholipour, G. Adamo, D. Cortecchia, et al., "Organometallic perovskite metasurfaces," *Adv. Mater.*, vol. 29, no. 9, 2017, Art no. 1604268.

[12] C. Zhang, S. Xiao, Y. Wang, et al., "Lead halide perovskite-based dynamic metasurfaces," Laser Photon. Rev., vol. 13, no. 1, 2019, Art no. 1900079, https://doi.org/10.1002/lpor.201900079.

[13] S. Makarov, A. Furasova, E. Tiguntseva, et al., "Halide-perovskite resonant nanophotonics," *Adv. Opt. Mater.*, vol. 7, no. 1, 2019, Art no. 1800784, https://doi.org/10.1002/adom.201800784.

[14] K. Wang, G. Li, S. Wang, et al., "Dark-field sensors based on organometallic halide perovskite microlasers," *Adv. Mater.*, vol. 30, no. 32, 2018, Art no. 1801481.

[15] A. S. Berestennikov, P. M. Voroshilov, S. V. Makarov, and Y. S. Kivshar, "Active metaoptics and nanophotonics with halide perovskites," *Appl. Phys. Rev.*, vol. 6, no. 3, 2019, Art no. 031307.

[16] E. Y. Tiguntseva, K. L. Koshelev, A. D. Furasova, et al., *Single-particle Mie-resonant All-dielectric Nanolasers*, arXiv preprint arXiv:1905.08646, 2019.

[17] A. Balena, A. Perulli, M. Fernandez, et al., "Temperature dependence of the amplified spontaneous emission from $CsPbBr_3$ nanocrystal thin films," *J. Phys. Chem. C*, vol. 122, no. 10, pp. 5813–5819, 2018.

[18] M. L. De Giorgi, F. Krieg, M. V. Kovalenko, and M. Anni, "Amplified spontaneous emission threshold reduction and operational stability improvement in $CsPbBr_3$ nanocrystals films by hydrophobic functionalization of the substrate," *Sci. Rep.*, vol. 9, no. 1, pp. 1–10, 2019.

[19] K. Wang, S. Wang, S. Xiao, and Q. Song, "Recent advances in perovskite micro-and nanolasers," *Adv. Opt. Mater.*, vol. 6, no. 18, 2018, Art no. 1800278.

[20] A. S. Polushkin, E. Y. Tiguntseva, A. P. Pushkarev, and S. V. Makarov, "Single-particle perovskite lasers: from material properties to cavity design," *Nanophotonics*, vol. 9, no. 3, pp. 599–610, 2020.

[21] Q. Liao, K. Hu, H. Zhang, X. Wang, J. Yao, and H. Fu, "Perovskite microdisk microlasers self-assembled from solution," *Adv. Mater.*, vol. 27, no. 22, pp. 3405–3410, 2015.
[22] P. J. Cegielski, A. L. Giesecke, S. Neutzner, et al., "Monolithically integrated perovskite semiconductor lasers on silicon photonic chips by scalable top-down fabrication," *Nano Lett.*, vol. 18, no. 11, pp. 6915–6923, 2018.
[23] W. Tian, H. Zhou, and L. Li, "Hybrid organic–inorganic perovskite photodetectors," *Small*, vol. 13, no. 41, 2017, Art no. 1702107.
[24] Y. Jia, R. A. Kerner, A. J. Grede, B. P. Rand, and N. C. Giebink, "Factors that limit continuous-wave lasing in hybrid perovskite semiconductors," *Adv. Opt. Mater.*, vol. 8, no. 2, 2020, Art no. 1901514.
[25] X. Wang, X. Zhuang, S. Yang, et al., "High gain submicrometer optical amplifier at near-infrared communication band," *Phys. Rev. Lett.*, vol. 115, no. 2, 2015, Art no. 027403.
[26] H. K. Yu and J. L. Lee, "Growth mechanism of metal-oxide nanowires synthesized by electron beam evaporation: a self-catalytic vapor–liquid–solid process," *Sci. Rep.*, vol. 4, p. 6589, 2014.
[27] G. Meng, T. Yanagida, K. Nagashima, et al., "Impact of preferential indium nucleation on electrical conductivity of vapor–liquid–solid grown indium–tin oxide nanowires," *J. Am. Chem. Soc.*, vol. 135, no. 18, pp. 7033–7038, 2013.
[28] L. Markov, A. Pavluchenko, I. Smirnova, and S. Pavlov, "Study of the effective refractive index profile in self-assembling nanostructured ITO films," *Semiconductors*, vol. 52, no. 10, pp. 1349–1356, 2018.
[29] A. P. Pushkarev, V. I. Korolev, D. I. Markina, et al., "A few-minute synthesis of $CsPbBr_3$ nanolasers with a high quality factor by spraying at ambient conditions," *ACS Appl. Mater. Interfaces*, vol. 11, no. 1, pp. 1040–1048, 2019.
[30] J. Summers, T. Vallaitis, P. Evans, et al., "Monolithic InP-based coherent transmitter photonic integrated circuit with 2.25 Tbit/s capacity," *Electron. Lett.*, vol. 50, no. 16, pp. 1150–1152, 2014.
[31] F. Vollmer and S. Arnold, "Whispering-gallery-mode biosensing: label-free detection down to single molecules," *Nat. Methods*, vol. 5, no. 7, p. 591, 2008.
[32] M. Lax, "Classical noise. V. Noise in self-sustained oscillators," *Phys. Rev.*, vol. 160, no. 2, p. 290, 1967.
[33] R. Slusher, A. Levi, U. Mohideen, S. McCall, S. Pearton, and R. Logan, "Threshold characteristics of semiconductor microdisk lasers," *Appl. Phys. Lett.*, vol. 63, no. 10, pp. 1310–1312, 1993.
[34] A. Maslov and C. Z. Ning, "Reflection of guided modes in a semiconductor nanowire laser," *Appl. Phys. Lett.*, vol. 83, no. 6, pp. 1237–1239, 2003.
[35] Y. Fu, H. Zhu, C. C. Stoumpos, et al., "Broad wavelength tunable robust lasing from single-crystal nanowires of cesium lead halide perovskites ($CsPbX_3$, X = Cl, Br, I)," *ACS Nano*, vol. 10, no. 8, pp. 7963–7972, 2016.
[36] H. Zhou, S. Yuan, X. Wang, et al., "Vapor growth and tunable lasing of band gap engineered cesium lead halide perovskite micro/nanorods with triangular cross section," *ACS Nano*, vol. 11, no. 2, pp. 1189–1195, 2016.
[37] X. Wang, M. Shoaib, X. Wang, et al., "High-quality in-plane aligned $CsPbX_3$ perovskite nanowire lasers with composition-dependent strong exciton–photon coupling," *ACS Nano*, vol. 12, no. 6, pp. 6170–6178, 2018.
[38] H. Yu, Xu X., Liu H., et al. Waterproof cesium lead bromide perovskite lasers and their applications in solution. ACS Nano vol. 14, no. 1, pp. 552–558, 2019.
[39] C. Huang, C. Zhang, S. Xiao, et al., "Ultrafast control of vortex microlasers," *Science*, vol. 367, no. 6481, pp. 1018–1021, 2020.
[40] N. Zhang, W. Sun, S. P. Rodrigues, et al., "Highly reproducible organometallic halide perovskite microdevices based on top-down lithography," *Adv. Mater.*, vol. 29, no. 15, 2017, Art no. 1606205, https://doi.org/10.1002/adma.201606205.
[41] A. Y. Zhizhchenko, P. Tonkaev, D. Gets, et al., "Light-emitting nanophotonic designs enabled by ultrafast laser processing of halide perovskites," *Small*, 2020, Art no. 2000410, https://doi.org/10.1002/smll.202000410.
[42] L. Markov, I. Smirnova, A. Pavluchenko, M. Kukushkin, D. Zakheim, and S. Pavlov, "Technique for forming ITO films with a controlled refractive index," *Semiconductors*, vol. 50, no. 7, pp. 984–988, 2016.
[43] E. Y. Tiguntseva, D. G. Baranov, A. P. Pushkarev, et al., "Tunable hybrid fano resonances in halide perovskite nanoparticles," *Nano Lett.*, vol. 18, no. 9, pp. 5522–5529, 2018.
[44] A. M. Leguy, P. Azarhoosh, M. I. Alonso, et al., "Experimental and theoretical optical properties of methylammonium lead halide perovskites," *Nanoscale*, vol. 8, no. 12, pp. 6317–6327, 2016.

Supplementary material: The online version of this article offers supplementary material (https://doi.org/10.1515/nanoph-2020-0207).